Optical and Resonant X-Ray Diffraction Studies Confirm a SmC^*_{FI2}-SmC^* Liquid Crystal Phase Sequence Reversal

S. T. Wang,[1] Z. Q. Liu,[1] B. K. McCoy,[1] R. Pindak,[2] W. Caliebe,[2] H. T. Nguyen,[3] and C. C. Huang[1]

[1]*School of Physics and Astronomy, University of Minnesota, Minneapolis, Minnesota 55455, USA*

[2]*NSLS, Brookhaven National Laboratory, Upton, New York 11973, USA*

[3]*Centre de Recherche Paul Pascal, CNRS, Université Bordeaux I, Avenue A. Schweitzer, F-33600 Pessac, France*

(Received 15 December 2005; published 6 March 2006)

Employing both null transmission ellipsometry and resonant x-ray diffraction, we confirmed the SmC^*_{FI2}-SmC^* phase sequence reversal in one liquid crystal compound and specially prepared binary mixtures. This phase sequence reversal was predicted by two recent theoretical advances. Moreover, the temperature range for the SmC^*_{FI2} phase increases significantly in the mixture suggesting that such a phase sequence may exist in other compounds.

DOI: 10.1103/PhysRevLett.96.097801 PACS numbers: 61.30.Gd, 77.84.Nh

The chiral smectic liquid crystal phases have drawn considerable attention in condensed matter physics not only for their potential applications in electro-optic devices, but also for their numerous phases, which provide good candidates to study the molecular interactions. To date, at least five different chiral smectic phases have been found: SmC^*_α, SmC^*, SmC^*_{FI2}, SmC^*_{FI1}, and SmC^*_A. The molecules in these SmC^* variant phases are all uniformly tilted from the layer normal but different interlayer orientational structures yield different phases [1,2]. For example, the SmC^*_A phase has a 2-layer structure with the tilt orientation alternating between successive layers. These phases have been studied extensively using different experimental tools, such as optical probes [3–6] and resonant x-ray diffraction (RXRD) [7,8]. Recently, phenomenological models [9,10] and microscopic advances [11,12] have been developed and refined to describe the stability and detailed structure of these phases. In particular, the SmC^*_{FI2} and SmC^*_{FI1} phases were shown to be biaxial phases with, respectively, 4- and 3-layer periodicities of their molecular tilt directions.

To date, upon cooling almost all the antiferroelectric liquid crystal compounds display the following phase sequence: SmA-SmC^*_α-SmC^*-SmC^*_{FI2}-SmC^*_{FI1}-SmC^*_A [13]. Laux *et al.* have reported an unusual phase sequence upon cooling in 10OHFBBB1M7 (10OHF), namely, SmC^*_α-SmC^*_{FI}-SmC^*. This unusual phase sequence is one of two possible cases [14,15] out of a few hundreds of antiferroelectric liquid crystal compounds that have been studied. In the other case [15], the SmC^*_{FI} phase is not stable; it appears only in a narrow temperature range upon very slow cooling. From their optical microscopy studies, they were unable to determine the structure of the intermediate SmC^*_{FI} phase. We have conducted detailed studies using null transmission ellipsometry (NTE) and RXRD on 10OHF and/or specially prepared binary mixtures of 10OHF and 9OTBBB1M7 (C9). The SmC^*_{FI} phase is unambiguously determined to be SmC^*_{FI2}, indicating a reversal of the usually observed phase sequence of the SmC^* and SmC^*_{FI2} phases. Moreover, the temperature range for the SmC^*_{FI2} phase increases rapidly with increasing concentration of C9. Nonetheless, two recent theoretical advances concerning these SmC^* variant phases [10,11] indicate that this phase sequence occurs as model parameters are varied monotonically. This suggests that this phase sequence reversal may be common, existing in other compounds.

The details of our NTE experimental setup have been described elsewhere [16]. The freestanding film geometry is used in the setup. If the film has net polarization in the film plane, the polarization will align with the electric field (E). Acquiring the ellipsometric parameters Δ and Ψ as a function of the E orientation (denoted by an angle α), we can infer the optical symmetry of the phase and obtain the molecular arrangement in the film. Ellipsometric runs were performed by ramping temperature up and down under two orientations of E. In our NTE, Δ measures the phase difference between the $\hat{p}$ and $\hat{s}$ components of the incident light necessary to produce linearly polarized transmitted light. Ψ describes the polarization angle of this linearly polarized light.

The RXRD experiment was conducted at beam line X19A at the National Synchrotron Light Source. The incident x-ray energy was set to the maximum of the fluorescence spectrum of C9 at $E_0 = 2.471$ keV for the RXRD measurements. The diffraction was done along the Q_z reciprocal space direction, where z denotes the layer normal direction. To reduce absorption by the air, the sample chamber and all the x-ray flight paths were flushed with helium. The setup details can be found in a previous paper [7].

Figure 1 shows Δ as a function of temperature for a 60-layer film of 10OHF at $\alpha = 90°$ and $\alpha = 270°$ upon cooling at a ramping rate of 70 mK/min. There are four distinct regions which correspond to four different phases. Above T_1, the film was in the SmA phase. Because of the

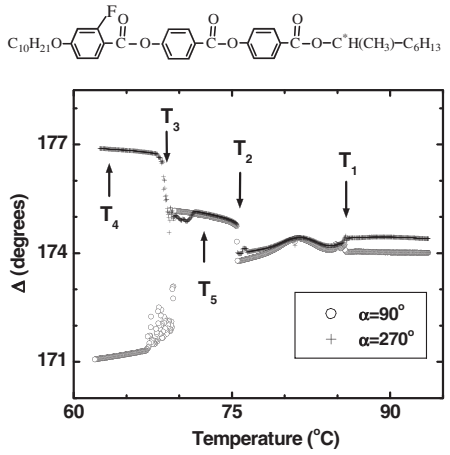

FIG. 1. Δ as a function of temperature for a 60-layer film of 10OHF under $|E| = 14.3$ V/cm at $\alpha = 90°$ (circles) and $\alpha = 270°$ (crosses) upon cooling. The ramping rate was 70 mK/min. T_1, T_2, and T_3 are the transition temperatures through the SmA-SmC^*_α-SmC^*_{FI2}-SmC^* phase sequence. The chemical structure of 10OHF is shown at the top.

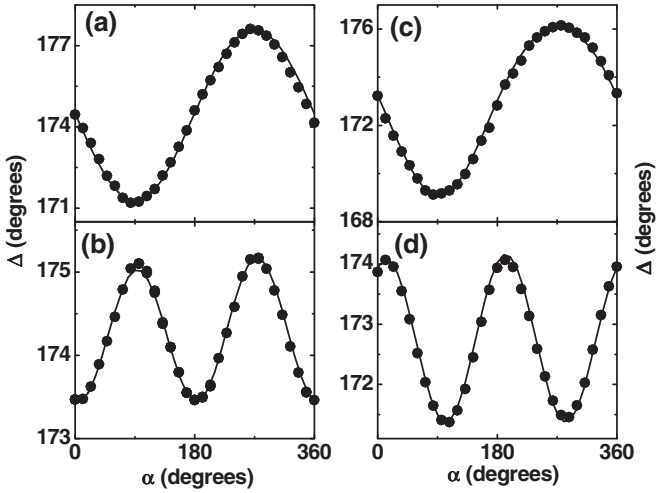

FIG. 2. Δ as a function of α for a 60-layer film of 10OHF in the (a) SmC^* phase at 63.7 °C and (b) SmC^*_{FI2} phase at 72.2 °C, and for a 56-layer film of the mixture $(10OHF)_{0.75}(C9)_{0.25}$ in the (c) SmC^* phase at 50.0 °C and (d) SmC^*_{FI2} phase at 65.8 °C. The dots are the data and the lines are the simulation results. The fitting parameters are $n_e = 1.635$, $n_o = 1.483$, and $d = 39.0$ Å for (a),(b), and $n_e = 1.645$, $n_o = 1.485$, and $d = 38.9$ Å for (c),(d). Other parameters are as follows: (a) $\theta = 15.6°$, $p = 0.57$ μm; (b) $\theta = 14.2°$, $p = 1.25$ μm, $\delta = 18°$; (c) $\theta = 17.5°$, $p = 0.60$ μm; (d) $\theta = 17°$, $p = 3.1$ μm, $\delta = 24°$. To save space, only Δ vs α data are shown.

surface enhanced ordering, the surface layers were tilted in the SmA phase so Δ_{90} was not equal to Δ_{270}. Both Δ_{90} and Δ_{270} display oscillation between T_1 and T_2, which is characteristic of the SmC^*_α phase [17]. The previously undetermined SmC^* variant phase existed between T_2 and T_3. Below T_3 was the SmC^* phase, characterized by the jumps of Δ_{90} and Δ_{270} because of the biaxiality change. Δ and Ψ as a function of α were measured at T_4 and T_5 to confirm the structures of the phases as, respectively, the SmC^* and SmC^*_{FI2} phases. The data are shown in Figs. 2(a) and 2(b). The Δ curve in Fig. 2(a) is a typical curve for the SmC^* phase, which has a minimum at Δ_{90} and a maximum at Δ_{270} [18]. In Fig. 2(b), the data have a 180° rotation symmetry, which indicates that this phase is potentially the SmC^*_{FI2} phase instead of the SmC^*_{FI1} phase because the 3-layer periodicity in SmC^*_{FI1} does not result in 180° rotation symmetry [5].

Simulation results have been obtained using the 4×4 matrix method with the film being modeled as a stratified medium [19]. The required parameters for modeling the film in the smectic phases are the number of smectic layers (N), the layer spacing (d), the indices of refraction [n_e and n_o along the molecular long axis ($\hat{n}$) and perpendicular to $\hat{n}$, respectively], the tilt angle of the molecules (θ), and the optical pitch (p). For the SmC^*_{FI2} phase, the distorted clock model is used to fit the data so the distortion angle (δ) is an additional parameter [5]. The simulation parameters N, n_e, n_o, and d used for both the SmC^* and SmC^*_{FI2} phases were obtained by preparing and measuring Δ and Ψ for 70 films in the SmA phase [20]. The other parameters θ, p, and δ, listed in the caption of Fig. 2, were determined by fitting the data. In fact, the molecular arrangements of either the SmC^*_{FI2} or SmC^*_A phases can describe our ellipsometric data obtained in this intermediate phase; because the optical wavelength is much larger than the layer periodicity (2-layer and 4-layer), our ellipsometric data cannot distinguish these two phases. However, the phase diagram shown in Fig. 3(a) suggests that the intermediate phase should be a SmC^*_{FI2} phase instead of SmC^*_A phase because the phase sequence SmC^*_α-SmC^*_{FI2}-SmC^* following line 2 occurs as model parameters a_1 and a_2 are varied monotonically. Since SmC^* ($a_1 < 0$) is usually in higher temperature than SmC^*_A ($a_1 > 0$), it is reasonable that the magnitude of a_1 decreases with decreasing temperature as line 2 indicates. This temperature dependence of a_1 has been confirmed in previous studies [9,21].

In contrast to conventional x-ray diffraction, RXRD can probe the orientation of the molecules in each layer. Consequently, extra resonant satellites ($m = \pm 1, \pm 2$) of principle peaks ($l = 1, 2, \ldots$) can be detected at positions $Q_z/Q_o = l + m(1/n \pm \epsilon)$ in SmC^* variant phases having n-layer periodicity. Here $\epsilon = d/p$. Thus, RXRD is the best way to determine whether the intermediate phase is a SmC^*_{FI2} phase with a 4-layer structure. To facilitate such a study, binary mixtures of $(10OHF)_{1-y}(C9)_y$, with $y = 0.10, 0.25, 0.375$, and 0.50, were prepared [22]. Employing NTE, we have obtained the phase diagram of this binary mixture system as shown in Fig. 3(b). To our great surprise, the temperature window for the intermediate phase increases rapidly with the concentration of C9. For $y = 0.50$, the film ruptured at 52.0 °C before the lower temperature phase could be identified; the intermediate phase

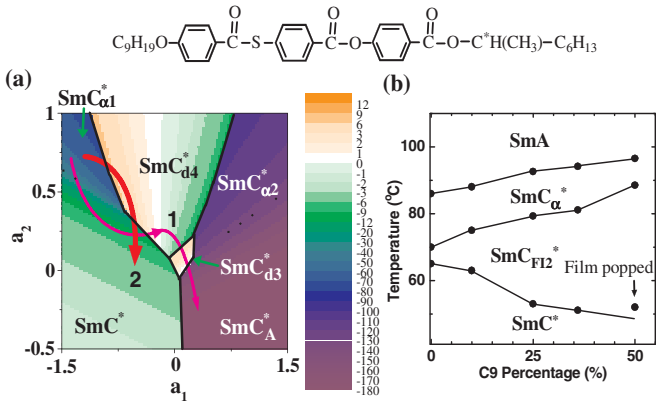

FIG. 3 (color online). (a) Phase diagram obtained from simulations of a free energy having five expansion terms: three effective interlayer interactions and chiral and steric interaction terms [10]. a_1 and a_2 are coefficients of the nearest- and next-nearest-neighbor interaction terms. The parameters of the three other terms are set to constants in this diagram. SmC^*_{d4} and SmC^*_{d3} are phases having 4- and 3-layer unit cells with distorted clock structures, which are similar to SmC^*_{FI2} and SmC^*_{FI1} phases, respectively. The color scale represents the overall helical pitch of the structure. Line 1 (magenta) represents the phase sequence SmC^*_α-SmC^*-SmC^*_{FI2}-SmC^*_{FI1}-SmAC^*_A upon cooling found in the majority of antiferroelectric liquid crystal compounds. Line 2 (red) shows the phase sequence reversal SmC^*_α-SmC^*_{FI2}-SmC^* found in 10OHF and its binary mixtures. (b) The phase diagram of the $(10OHF)_{1-y}(C9)_y$ mixtures with C9. The dots are experimental data from our NTE measurements acquired in cooling runs except for $y = 0.10$ [25]. The chemical structure of C9 is shown at the top.

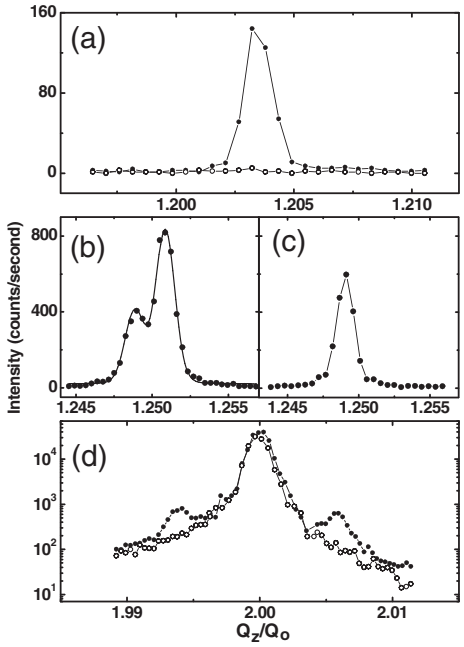

FIG. 4. X-ray intensity scans in the (a) SmC^*_α phase at 81.4 °C, the SmC^*_{FI2} phase at (b) 61.0 °C and (c) 76.5 °C, and (d) the SmC^* phase at 45.3 °C of the mixture $(10OHF)_{0.75}(C9)_{0.25}$. The dots and open circles are the data at resonant energy E_0 and nonresonant energy $E_0 + 10$ eV, respectively. The solid lines in (b) are the simulated resonant peaks.

was stable over more than 30 K. Among the mixtures, $y = 0.25$ was selected for detailed NTE and RXRD studies. As shown in Figs. 2(c) and 2(d), the Δ vs α data obtained at 50.0 °C and 65.8 °C demonstrate the SmC^* and SmC^*_{FI2} phases, respectively. Compared to Fig. 2(b), there is a $\sim 90°$ shift of the data in Fig. 2(d). This is because the helical pitches and distortion angles in the SmC^*_{FI2} phase of the mixture and pure 10OHF are very different so that the net polarization direction in one case is in the average molecular tilt plane and in the other case perpendicular to the plane.

RXRD was conducted on the $(10OHF)_{0.75}(C9)_{0.25}$ mixture. We scanned for resonant peaks at different temperatures and identified the SmC^*_α, SmC^*_{FI2}, and SmC^* phases sequentially upon cooling. Resonant peaks of these three phases are shown in Fig. 4. Figure 4(a) displays the ($l = 1$, $m = 1$) resonant peak of the SmC^*_α phase at 81.4 °C. From the positions of the (001) main peak and ($l = 1$, $m = \pm 1$) resonant peaks, the incommensurate helical pitch of the SmC^*_α phase was determined to be 4.92 layers, consistent with the pitch measured by our optical method for pure 10OHF [21].

Since the intermediate phase of this mixture has a wide temperature window ($\sim$25 K), we scanned the resonant peaks at six temperatures in this window. Only 1/4 order resonant peaks were observed, which confirmed that the intermediate phase was the SmC^*_{FI2} phase with a 4-layer structure. Figure 4(b) shows the resonant peaks of the SmC^*_{FI2} phase at 61.0 °C at $Q_z/Q_o = 1.25$. By fitting the data using the distorted clock model [5,23], we found that the distortion angle of the biaxial SmC^*_{FI2} phase is $23 \pm 3°$ and the optical pitch is ~ 3.9 μm. Both values are in good agreement with those obtained from NTE.

Within our experimental resolution [24], we also found that the 1/4 order resonant peak at the high temperature end of the SmC^*_{FI2} window was a single peak as shown in Fig. 4(c). Thus the 4-layer superstructure at high temperatures can have either a simple clock arrangement or a distorted clock structure with a very long overall optical pitch. While the first one is an optically uniaxial phase, the second one is a biaxial phase. Subsequently, our detailed optical measurements yielded similar Δ and Ψ vs α throughout the SmC^*_{FI2} phase window, supporting biaxial properties of this phase. In addition, simulations of the Δ and Ψ vs α data and the increasing split width of the resonant peaks upon cooling yield that the helicoidal pitch decreases as temperature decreases in the SmC^*_{FI2} phase. This is one clear demonstration that NTE and RXRD are complementary probes in acquiring molecular arrangements of SmC^* variant phases. Here the combination of NTE and RXRD significantly enhances our capability to

unambiguously determine that the intermediate phase is the SmC^*_{FI2} phase with a distorted clock structure.

After the SmC^*_{FI2} phase was identified, upon further cooling, the satellite resonant peaks of the SmC^* phase were found. A typical scan through the (002) Bragg peak and the corresponding $m = \pm 1$ satellite peaks of the SmC^* phase at 45.3 °C is shown in Fig. 4(d). A scan having incident energy $E_0 + 10$ eV, showing no resonant peaks, is superimposed. From the satellite peak positions, the optical pitch was determined to be 0.66 μm, also consistent with the pitch value (0.60 μm) obtained from optical measurements. It is very interesting to see that the optical pitch drops significantly from the SmC^*_{FI2} phase to the SmC^* phase.

RXRD has confirmed the SmC^*_α-SmC^*_{FI2}-SmC^* phase sequence in the $(10\text{OHF})_{0.75}(\text{C9})_{0.25}$ mixture. By extrapolation, we can conclude that this unusual phase sequence also exists in pure 10OHF. Since the 4-layer structure is immediately below the SmC^*_α phase upon cooling, it is understandable that the short helical pitch in the SmC^*_α phase of 10OHF decreases from 6.5 layers to 5.5 layers upon cooling [21]. Employing NTE, we also checked the phase sequences of several homologous compounds, 12-, 11-, and 9-OHF, and found that their phase sequences all follow the usual phase sequence. Why 10OHF is so unique to exhibit the unusual phase sequence among the homologous series still remains a great puzzle. Usually the intermediate phase in an unusual phase sequence is an unstable phase, which may disappear upon doping. However, the SmC^*_{FI2} phase in the $(10\text{OHF})_{1-y}(\text{C9})_y$ mixture is very stable and its temperature window expands rapidly with increasing y, squeezing out the SmC^* phase. Moreover, the contour for the SmC^*_α-SmC^*_{FI2}-SmC^* phase sequence through simulated phase diagrams in both Ref. [10] [line 2 in Fig. 3(a)] and [11] is somewhat simpler than the one for the SmC^*_α-SmC^*-SmC^*_{FI2}-SmC^*_{FI1}-SmC^*_A phase sequence [line 1 in Fig. 3(a)]. These facts strongly suggest that the SmC^*_α-SmC^*_{FI2}-SmC^* phase sequence may not be so unusual and may exist in other compounds. Thus special attention will be paid to the data of various antiferroelectric liquid crystal compounds to identify any possible deviation from the usual phase sequence. Recently, Hamaneh and Taylor developed a model that incorporated long-range interlayer interactions to explain all the SmC^* variant phases [11]. The phase diagram that results from the theory can explain the usual phase sequence as well as the reversed phase sequence, which occurs as one of two model parameters is varied monotonically but very slowly. This theory also predicts a new phase with a 6-layer periodicity, which is supposed to appear between the SmC^* and SmC^*_{FI2} phases as temperature varies. If this new phase does exist experimentally, some new interesting phase sequences will be observed. Identifying the different possible variations of phase sequences is an important feature of the SmC^* variant phases that needs to be explained by theoretical models.

Work at the National Synchrotron Light Source was supported by the U.S. Department of Energy. The research was supported in part by the National Science Foundation, Solid State Chemistry Program under Grant No. DMR-0106122.

[1] R. B. Meyer *et al.*, J. Phys. (Paris), Lett. **36**, L69 (1975).
[2] A. Fukuda *et al.*, J. Mater. Chem. **4**, 997 (1994).
[3] Y. Galerne and L. Liebert, Phys. Rev. Lett. **66**, 2891 (1991).
[4] Ch. Bahr and D. Fliegner, Phys. Rev. Lett. **70**, 1842 (1993).
[5] P. M. Johnson *et al.*, Phys. Rev. Lett. **84**, 4870 (2000).
[6] D. Konovalov *et al.*, Phys. Rev. E **64**, 010704(R) (2001).
[7] P. Mach *et al.*, Phys. Rev. E **60**, 6793 (1999).
[8] L. S. Hirst *et al.*, Phys. Rev. E **65**, 041705 (2002).
[9] M. Cěpič and B. Zěkš, Phys. Rev. Lett. **87**, 085501 (2001).
[10] D. A. Olson *et al.*, Phys. Rev. E **66**, 021702 (2002).
[11] M. B. Hamaneh and P. L. Taylor, Phys. Rev. Lett. **93**, 167801 (2004); Phys. Rev. E **72**, 021706 (2005).
[12] A. V. Emelyanenko and M. A. Osipov, Phys. Rev. E **68**, 051703 (2003).
[13] Some of the phases may be missing for a given compound.
[14] V. Laux *et al.*, Liq. Cryst. **27**, 81 (2000).
[15] V. Faye *et al.*, Liq. Cryst. **21**, 485 (1996).
[16] D. A. Olson *et al.*, Liq. Cryst. **29**, 1521 (2002).
[17] P. M. Johnson *et al.*, Phys. Rev. Lett. **83**, 4073 (1999).
[18] S. T. Wang *et al.*, Liq. Cryst. **32**, 609 (2005).
[19] D. W. Berreman, J. Opt. Soc. Am. **62**, 502 (1972).
[20] C. C. Huang *et al.*, Phys. Rev. E **69**, 041702 (2004).
[21] A. Cady *et al.*, Phys. Rev. E **65**, 030701(R) (2002).
[22] The reason for choosing C9 as the dopant is that C9 has a very similar chemical structure and somewhat similar phase sequence to those of 10OHF. Its phase sequence is SmA(114.5 °C)SmC^*_α(109.2 °C)SmC^*_{FI2}(83.5 °C)SmC^*_A.
[23] A.-M. Levelut and B. Pansu, Phys. Rev. E **60**, 6803 (1999).
[24] The input and output vertical slits are set to 0.05 mm and horizontal slits are 0.5 mm wide. In principle, we can further reduce the vertical slit size to resolve the split peak in the high temperature window of the SmC^*_{FI2} phase. The reduction in scattered x-ray photon intensity may make such an approach time-consuming and impractical.
[25] The $y = 0.10$ mixture shows only the unusual phase sequence upon heating. All other mixtures show the unusual phase sequence upon both heating and cooling; the temperature range for the intermediate phase of heating runs is narrower than that of cooling runs.